*5174–5189* *Nucleic Acids Research, 2016, Vol. 44, No. 11* *Published online 3 March 2016*
*doi: 10.1093/nar/gkw142*

# Local potentiation of stress-responsive genes by upstream noncoding transcription

**Naomichi Takemata[1], Arisa Oda[1], Takatomi Yamada[2], Josephine Galipon[3], Tomoichiro Miyoshi[1], Yutaka Suzuki[4], Sumio Sugano[4], Charles S. Hoffman[5], Kouji Hirota[6] and Kunihiro Ohta[1,7,*]**

[1]Department of Life Sciences, The University of Tokyo, Meguro-ku, Tokyo 153-8902, Japan, [2]Department of Biological Sciences, Chuo University, Bunkyo-ku, Tokyo 112-8551, Japan, [3]Institute for Advanced Biosciences, Keio University, Tsuruoka, Yamagata 997-0035, Japan, [4]Department of Medical Genome Sciences, The University of Tokyo, Kashiwa, Chiba 277-8561, Japan, [5]Biology Department, Boston College, Chestnut Hill, MA 02467, USA, [6]Department of Chemistry, Tokyo Metropolitan University, Hachi-Ohji, Tokyo 192-0397, Japan and [7]Department of Biological Sciences, The University of Tokyo, Bunkyo-ku, Tokyo 113-0033, Japan

Received November 22, 2015; Revised February 22, 2016; Accepted February 25, 2016

## ABSTRACT

**It has been postulated that a myriad of long noncoding RNAs (lncRNAs) contribute to gene regulation. In fission yeast, glucose starvation triggers lncRNA transcription across promoter regions of stress-responsive genes including *fbp1* (fructose-1,6-bisphosphatase1). At the *fbp1* promoter, this transcription promotes chromatin remodeling and *fbp1* mRNA expression. Here, we demonstrate that such upstream noncoding transcription facilitates promoter association of the stress-responsive transcriptional activator Atf1 at the sites of transcription, leading to activation of the downstream stress genes. Genome-wide analyses revealed that ∼50 Atf1-binding sites show marked decrease in Atf1 occupancy when cells are treated with a transcription inhibitor. Most of these transcription-enhanced Atf1-binding sites are associated with stress-dependent induction of the adjacent mRNAs or lncRNAs, as observed in *fbp1*. These Atf1-binding sites exhibit low Atf1 occupancy and high histone density in glucose-rich conditions, and undergo dramatic changes in chromatin status after glucose depletion: enhanced Atf1 binding, histone eviction, and histone H3 acetylation. We also found that upstream transcripts bind to the Groucho-Tup1 type transcriptional corepressors Tup11 and Tup12, and locally antagonize their repressive functions on Atf1 binding. These results reveal a new mechanism in which upstream noncoding transcription locally magnifies the specific activation of stress-inducible genes via counteraction of corepressors.**

## INTRODUCTION

Transcriptome analyses have revealed that eukaryotic genomes are pervasively transcribed to produce a myriad of long noncoding RNAs (lncRNAs) (1,2). At the beginning of their discovery, these transcripts were considered to be 'byproducts' or 'noise' resulting from stochastic transcription. However, it has been increasingly evident that a substantial number of these lncRNAs have diverse biological functions including transcriptional or post-transcriptional gene regulation, establishment of epigenetic marks, and organization of subnuclear structures (3). In addition, some lncRNAs also play pivotal roles in development and carcinogenesis (4).

lncRNAs have been suggested to regulate gene expression by recruiting or modulating transcriptional regulators such as Mediator, DNA-binding proteins, histone-modifying enzymes, and chromatin-remodeling complexes (3). Functional modulation of these factors by lncRNAs is often mediated through physical interactions. For example, many lncRNAs bind to the histone-modifying enzyme PRC2 (polycomb repressive complex 2), and recruit the complex to their target loci (5,6). It should be noted that PRC2 can promiscuously bind to diverse RNAs, and the mechanism by which the RNA–PRC2 interaction leads to locus-specific targeting of PRC2 is not fully understood (7). lncRNA transcription *per se* also plays roles in gene regulation. For instance, noncoding transcription influences expression of the overlapping genes by interfering with RNA polymerase II (Pol II) or by Pol II-dependent cotranscriptional modification of chromatin status (8–12).

*To whom corresponding should be addressed. Tel: +81 3 5465 8834; Fax: +81 3 5465 8834; Email: kohta@bio.c.u-tokyo.ac.jp
Present address: Tomoichiro Miyoshi, Department of Gene Mechanisms, Kyoto University, Sakyo-ku, Kyoto 606-8501, Japan.

lncRNA transcription occurs at various genomic locations, with a multitude of lncRNAs overlapping promoter regions of protein-coding genes (we hereafter refer to this feature as 'upstream lncRNA') (13–17). In general, upstream lncRNAs are either rapidly processed by RNA-degradation machinery or transcriptionally downregulated by a repressive chromatin configuration (18–22). Therefore, their effects are normally concealed. However, a number of studies have suggested that upstream lncRNA transcription participates in the regulation of adjacent genes (8,23–27). For example, in the budding yeast *Saccharomyces cerevisiae*, transcription of the lncRNA *SRG1* (*SER3* regulatory gene 1) through the *SER3* promoter results in phasing of nucleosomes in the promoter, leading to transcriptional silencing of the *SER3* gene (24,28). In humans, an upstream transcript named *ecCEBPA* (extra-coding *CEBPA*) activates the downstream overlapping gene *CEBPA* by locally inhibiting the DNA methyltransferase DNMT1 (27). Despite these findings, the mechanistic roles of upstream lncRNAs in gene regulatory processes are largely unknown.

In the fission yeast *Schizosaccharomyces pombe*, we previously identified a set of Pol II-dependent lncRNAs that originate from the promoter region of *fbp1* (fructose-1,6-bisphosphatase 1), a gene encoding a key enzyme for gluconeogenesis (29,30). We named these upstream noncoding transcripts 'mlonRNAs' (metabolic stress-induced long noncoding RNAs) (31). In glucose-rich medium, the longest version of mlonRNA (mlonRNA-a) is weakly transcribed upstream of a distal regulatory element named UAS1 (upstream activation site 1, Figure 1A) (32), while the antisense lncRNA *fbp1-as* is expressed from a 3′ region of the *fbp1* gene (14). On the other hand, in response to glucose starvation, *fbp1-as* is downregulated and shorter sense mlonRNAs (mlonRNA-b and -c) are in turn transcribed from the region between UAS1 and another regulatory element UAS2 (upstream activation site 2) (32). Such cascade-like transcription of mlonRNAs triggers a 5′ to 3′ stepwise chromatin conformation change in the *fbp1* promoter and subsequent robust induction of *fbp1* mRNA. Our recent RNA-sequencing (RNA-seq) analysis revealed that similar upstream lncRNAs are expressed near other stress-responsive genes upon glucose starvation (14).

The induction of *fbp1* is triggered specifically upon glucose starvation stress (33), which is regulated by several proteins. The stress-activated protein kinase Sty1/Spc1 activates *fbp1* expression via its effector Atf1, an ATF/CREB (activating transcription factor/cyclic AMP-responsive element binding) transcription factor that binds to UAS1 (32,34,35). The $C_2H_2$-type Zn finger activator Rst2 relocates into the nucleus in response to glucose depletion, and activates the mRNA transcription by binding to UAS2 (36,37). Other proteins such as the CCAAT-binding factor Php2–5 and the Groucho/Tup1-family global corepressors Tup11 and Tup12 are also involved in the regulation of *fbp1* expression (38–40). Elucidating how these factors and mlonRNA transcription collaborate to regulate *fbp1* expression would provide insight into the physiological role of upstream noncoding RNAs.

In this study, we demonstrate that the upstream noncoding transcription in some stress genes facilitates Atf1 binding to target sites, leading to histone acetylation, nucleosome eviction, and stress-dependent gene activation. The results also suggest that those upstream transcripts bind to Tup11 and Tup12 to antagonize their repressive functions on Atf1 binding.

## MATERIALS AND METHODS

### *pombe* strains

*S. pombe* strains used in this study are listed in Supplementary Table S1. In the *fbp1-CRE*Δ mutant, the *fbp1* sequence ranging from −1183 to −1125 (relative to the first 'A' of the ORF, other regions below are represented in the same way) was deleted. In the *fbp1-*$P_{bc}$Δ*::spacer* mutant, the *fbp1* region ranging from −1103 to −598 was replaced with a part of the *S. cerevisiae LEU2* ORF (from +56 to +561). For ectopic expression of mlonRNAs, the *fbp1* sequence (from −1671 to +1695) was cloned into the pREP2 plasmid. This vector was cut with PmaCI, and integrated into the *nmt1-gut2* locus by homologous recombination.

### Cell culture

Yeast cells were precultured at 30°C in YES medium (5 g/l yeast extract, 200 mg/l each of adenine, leucine, and histidine, 100 mg/l uracil, 30 g/l glucose) and cultured overnight in glucose-rich medium YER (5 g/l yeast extract, 100 mg/l adenine, 60 g/l glucose) until the concentration reached ∼2 × $10^7$ cells/ml. The sample of '0 min' was collected at this point. To induce glucose starvation, the rest of cell culture was transferred into low-glucose medium YED (5 g/l yeast extract, 100 mg/l adenine, 1 g/l glucose, 3% glycerol) and harvested at each time point as described previously (31).

To inhibit transcription, 1,10-phenanthroline monohydrate (Sigma-Aldrich) was dissolved in ethanol at a concentration of 100 mg/ml, and added to cell cultures immediately after the shift to YED medium at a final concentration of 100 μg/ml. Thiolutin (Wako) was dissolved in dimethyl sulfoxide (DMSO) at a concentration of 5 mg/ml, and added to cell cultures immediately after the shift to YED medium at a final concentration of 20 μg/ml. The same volume of ethanol or DMSO was added for mock treatment. Cells were harvested 15 min after the treatments.

### Northern blotting

Northern blotting was performed essentially as described previously (31). DNA probes were labeled with [α-$^{32}$P]-dCTP using Random Primer DNA Labeling Kit Ver.2.0 (Takara). The primers used for DNA probe synthesis are listed in Supplementary Table S2.

### Western blotting

Cells were collected by centrifugation and washed with distilled water. Cell pellets were resuspended in protein extraction buffer (50 mM Tris–HCl, 5 mM EDTA, 150 mM KCl, 10 mM $MgCl_2$, 10% glycerol, 0.2% NP-40, 1 mM dithiothreitol, 20 mM β-glycerophosphate, 0.1 mM $Na_3VO_4$, 1 mM phenylmethylsulfonyl fluoride) containing 1× Complete Protease Inhibitor (Roche), and disrupted with zirconia beads and Multibead Shocker (Yasui kikai,

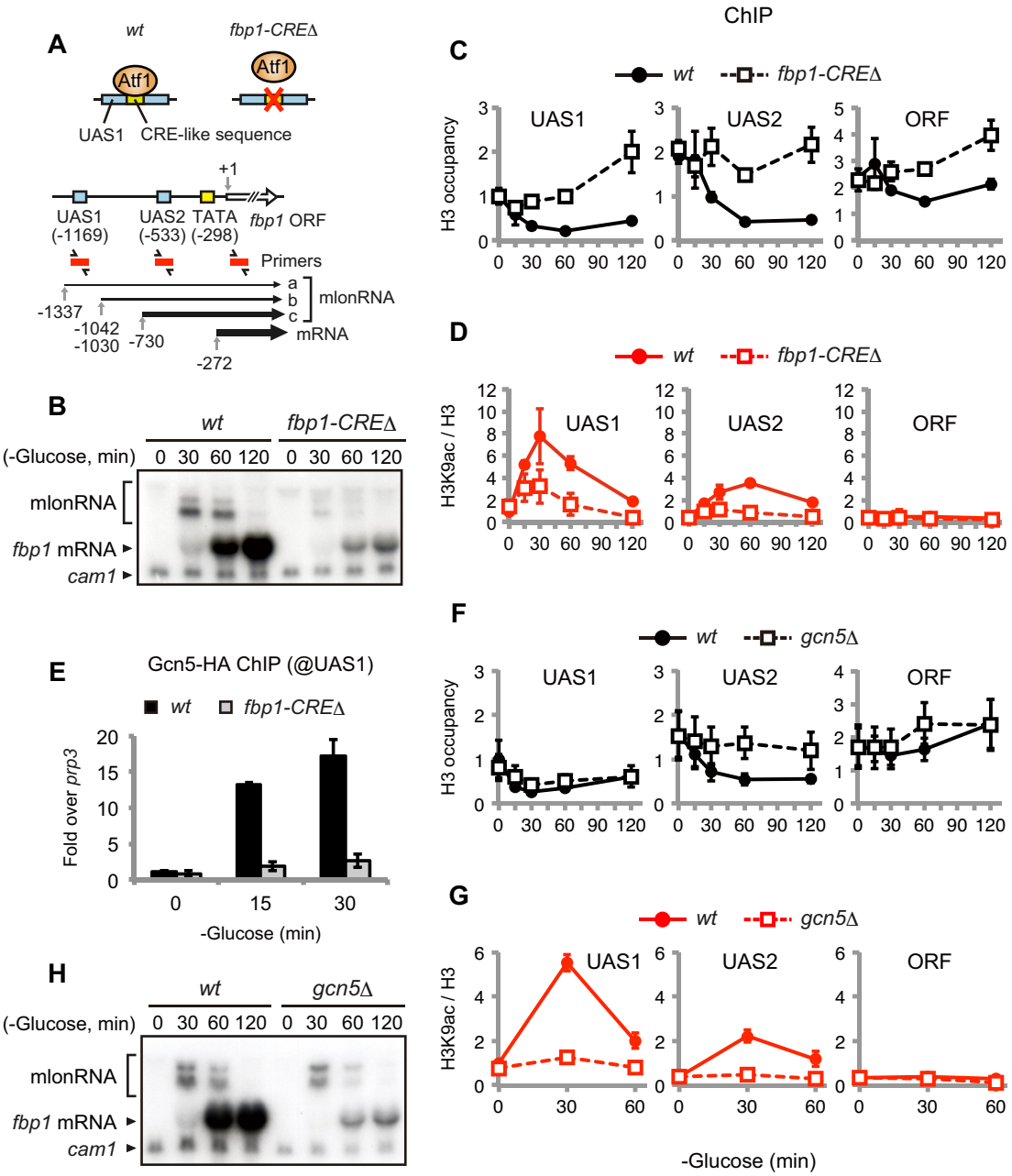


**Figure 1.** Binding of Atf1 promotes chromatin remodeling, histone acetylation, and RNA expression at *fbp1*. (**A**) Schematic representation of the *fbp1* locus and the *fbp1-CREΔ* mutation. Each number represents a location relative to the first 'A' of the *fbp1* ORF. Positions of the TATA element and the TSS of *fbp1* transcripts are according to previous publications (30,77). Red boxes represent the DNA regions amplified in ChIP-qPCR analyses. (**B**) Northern blot analysis of *fbp1* transcripts using a DNA probe for the *fbp1* ORF. *cam1* mRNA was used as an internal control. Note that the antisense transcript *fbp1-as* (14) is expressed very weakly and thus regarded as negligible in this study. Wild type (*wt*) and *fbp1-CREΔ* cells were used. (**C** and **D**) ChIP-qPCR analyses of histone H3 and H3K9ac. For H3 ChIP, signal of immunoprecipitated DNA (IP) was divided by that of whole cell extract (WCE). For H3K9ac, the IP/WCE value was divided by that of H3. Relative values are shown (the values of *wt*, 0 min at UAS1 were set to 1). Error bars represent standard deviations from three biological replicates. Note that some error bars are invisibly small. (**E**) ChIP-qPCR with an anti-HA antibody was carried out using cells expressing HA-tagged Gcn5. The IP/WCE value for the housekeeping gene *prp3* was used to define the background signal for normalization. Error bars represent standard deviations from three biological replicates. (**F** and **G**) ChIP-qPCR was performed as in Figure 1C and D. Error bars represent standard deviations from four (F) or three (G) biological replicates. Note that some error bars are invisibly small. (**H**) Northern blotting was performed as in Figure 1B.

Japan). Cell extracts were separated by SDS-PAGE. An antibody against Atf1 (33) or tubulin (Sigma, T5168) was used as a primary antibody. Detection was performed with horseradish peroxidase-conjugated anti-mouse IgG or anti-rabbit IgG (GE Healthcare).

### ChIP-qPCR

ChIP-qPCR was conducted essentially as described previously (14). Cell lysates were subjected to immunoprecipitation using antibodies for H3 (Abcam ab1791), H3K9ac (Millipore 07–352), the HA epitope (COVANCE 16B12), Atf1 (33), and the C-terminal region of Pol II (Millipore 05–623). Quantification was performed with Fast Real-Time PCR System 7300 or StepOnePlus (Applied Biosystems). Primer sets are listed in Supplementary Table S2. In the ChIP-qPCR experiments involving RNase treatment, immunoprecipitated material on antibody-conjugated beads was washed with Buffer 1 (50 mM HEPES–KOH, 140 mM NaCl, 1 mM EDTA, 1% Triton X-100, 0.1% sodium deoxycholate, pH 7.5), and resuspended in RNase-containing buffer (TE with 15 μl of RNase Cocktail™ Enzyme Mix [Life Technologies], or RNase H buffer [40 mM Tris–HCl, 4 mM $MgCl_2$] with 2 μl of RNase H [Takara]). Control samples were resuspended in buffers without RNase. After 15 min incubation at 37°C, beads washing and DNA extraction were conducted as in the conventional ChIP-qPCR protocol.

### ChIP-seq

Library preparation, sequencing and read mapping for H3K9ac ChIP-seq were performed according to Oda *et al.* (14). For Atf1 ChIP-seq, library preparation and sequencing were performed according to Ito *et al.* (41). ChIP-seq data for H3 was obtained from our previous study (14).

We used parse2wig2 and DROMPA (42) to generate genome-wide profiles of protein distribution. First, the *S. pombe* genome was divided into 10-bp bins, and the mapped reads in each bin were counted using parse2wig2 (options: -binsize 10 -nofilter). Because Atf1 is reported to be present at repetitive DNA regions (43), PCR bias filtering was omitted. Then, DROMPA was used for calculation of the enrichment ratio of immunoprecipitated DNA to input DNA for each bin, and for peak calling (options: -sw 300 –ethre 2.5 -ithre 2.5 -ratio1). Enrichment ratios were smoothed with a 300-bp size window, and normalized so that the genome average of enrichment ratio was equal to 1. This value was called 'occupancy'. Peak regions determined by DROMPA were further divided into subpeak regions using PeakSplitter (options: -c 3 -v 0.8 -f false) (44). For H3K9ac ChIP-seq, the H3 ChIP-seq data was used as input to estimate the modification levels per nucleosome. The ChIP-seq data are available at DDBJ (http://www.ddbj.nig.ac.jp) under accession numbers DRA004142 (Atf1 replicate 1), DRA004446 (Atf1 replicate 2), and DRA003541 (H3 and H3K9ac).

### ChIP-seq data analysis

We obtained Atf1 ChIP-seq datasets from two biological replicates (replicate 1 and 2). Since the two replicates showed high reproducibility (Supplementary Figures S5 and S10), the dataset of replicate 1 was used for analyses as a representative dataset. ChIP-seq profiles of H3 were from our previous study (14), and those of H3K9ac were derived from a single experiment. Unless otherwise stated, data analyses were performed using R software (http://www.r-project.org/). Analysis scripts are included in Supplementary Data. To compare Atf1 binding in glucose-starved cells (wild type, not treated with 1,10-phenanthroline) and in cells under a different condition, we first merged the lists of Atf1 peak regions obtained from the two conditions. For peaks detected in both conditions, we adopted the peak range defined in the former condition. Overlapping peaks were determined using ChIPpeakAnno version 3.2.2 (option: maxgap = 0) (45). Then, the bin average of Atf1 occupancy was calculated for each region (this value was defined as 'Atf1 occupancy' at each binding site), and this value was compared between the two conditions. H3 and H3K9ac levels at each Atf1-binding site were defined as the bin averages of the 1-kb region surrounding the Atf1 peak. The averages of protein distribution profiles around Atf1 peaks were shown as plots smoothed with a 150-bp size window.

### RNA-seq data analysis

For each Atf1-binding site, we estimated expression levels of RNA transcribed from the Atf1 peak within 1 kb. An Atf1 peak can be transcribed in two directions (sense and antisense), and they were analyzed individually. First, by utilizing our published RNA-seq datasets (14), the number of mapped RNA reads was counted for each base throughout the genome. These values were summed within the 1-kb regions using bedtools (46), and the sums were compared before and after 15 min of culture in low-glucose medium. A similar procedure was followed when estimating nocoding RNA expression around transcription-enhanced Atf1-binding sites, but RNA signals derived from protein-coding gene regions were subtracted. Transcription-enhanced sites that upregulated noncoding RNA expression (≥ 3-fold) from either of the two strands are listed in Supplementary Table S3. The RNA-seq data are available at DDBJ under accession number DRA002273.

### RNA immunoprecipitation

RNA immunoprecipitation was conducted as described previously (47) with some modifications. Cultures were fixed with 1% formaldehyde for 5 min, and the reaction was quenched with glycine. Cell pellets were resuspended in Buffer 1 containing 1xComplete Protease Inhibitor (Roche) and 40 U/ml RNasin (Promega), and disrupted with zirconia beads using Multi-Beads Shocker (Yasuikikai, Japan). Cell extracts were sonicated three times for 30 s at power 8 using Handy Sonic UR-20P (Tomy Seiko, Japan), and centrifuged (20,400 × g, 5 min, 4°C). Supernatants were incubated at 4°C for 3 h with anti-DYKDDDDK antibody (Wako) precoupled to Dynabeads Protein A (Life Technologies). Following two washes with Buffer 1 and one with DNase buffer (40 mM Tris–HCl, 8 mM $MgCl_2$), the beads were suspended in 100 μl of DNase buffer containing 25 U of DNase I (Takara), and incubated for 30 min

at 37°C. The beads were further washed once with Buffer 1′ (50 mM HEPES–KOH, 500 mM NaCl, 1 mM EDTA, 1% Triton X-100, 0.1% sodium deoxycholate, pH 7.5), three times with Buffer 2 (10 mM Tris–HCl, 1 mM EDTA, 250 mM LiCl, 0.5% NP-40, 0.5% sodium deoxycholate), and once with TE. The immunoprecipitates were eluted in 100 μL of Elution Buffer (20 mM Tris–HCl, 100 mM NaCl, 20 mM EDTA, 1% SDS) for 10 min at 65°C. Eluted samples were incubated with 1 μl of proteinase K (20 mg/ml, Life Technologies) for 1 h at 65°C. RNA was extracted by phenol/chloroform, precipitated with ethanol, and dissolved in RNase-free water. cDNAs were synthesized using PrimeScript RT Reagent Kit Perfect Real Time (Takara) according to the manufacturer's protocol. A mixture of oligo-dT primer and random hexamers was used. Real-time PCR was performed as for the ChIP experiment. Primer sets are listed in Supplementary Table S2.

## RESULTS

### Roles of Atf1 in chromatin regulation during glucose starvation

Deletion of the ATF/CREB family transcription factor Atf1 causes severe defects in chromatin remodeling at some stress genes including *fbp1* (30,48), suggesting critical roles of Atf1 in chromatin regulation. However, loss of Atf1 is assumed to cause secondary effects, since it can activate other stress genes as a transcriptional activator. We therefore examined effects of the deletion of the sole Atf1-binding *cis*-acting sequence, cAMP responsive element (CRE)-like sequence TGACGT (32) in UAS1 of the *fbp1* promoter (Figure 1A, referred to as '*fbp1-CRE*Δ mutation'). Northern blot analysis on cells shifted from 6% glucose to 0.1% glucose revealed that induction of *fbp1* mRNA and mlonRNAs upon glucose starvation was severely impaired in *fbp1-CRE*Δ cells (Figure 1B).

We then examined nucleosome density along the *fbp1* upstream sites (UAS1 and UAS2) and a 5′ site of the *fbp1* open reading frame (ORF) in *fbp1-CRE*Δ cells by chromatin immunoprecipitation-quantitative PCR (ChIP-qPCR) using an antibody against histone H3 (Figure 1A and C). After glucose depletion, H3 density in wild type was decreased more than two-fold at UAS1 and UAS2, but to a smaller extent in the ORF (Figure 1C). On the other hand, in *fbp1-CRE*Δ cells, the reduction of H3 density was not observed (H3 density at UAS1 was even increased at 120 minutes).

We further analyzed acetylation of Lys9 on histone H3 (H3K9ac) in this region by ChIP-qPCR assays, since Atf1 can recruit the histone acetyltransferase Gcn5 (49,50). As shown in Figure 1D, the ratio of H3K9ac to H3 density transiently increased at UAS1 and UAS2 after glucose depletion in wild type, whereas this response was almost absent in *fbp1-CRE*Δ. We also confirmed that human influenza hemagglutinin (HA)-tagged Gcn5 recruitment to UAS1 was dependent on the CRE-like sequence in UAS1 (Figure 1E). *gcn5Δ* cells exhibited defects in histone eviction, H3K9 acetylation and mRNA expression at the *fbp1* locus (Figure 1F–H). In contrast to *fbp1-CRE*Δ, the *gcn5*Δ mutation impaired histone eviction at UAS2 but not at UAS1. This difference may explain why mlonRNA expression was decreased in *fbp1-CRE*Δ cells but apparently not in *gcn5*Δ cells. Altogether, these data point towards a role of Atf1 as a primary regulator of chromatin disassembly and histone modification at the *fbp1* locus.

### Upstream noncoding transcription comprises a self-enhancing circuit of Atf1 binding

Upstream noncoding transcription in response to glucose starvation is associated with chromatin disassembly along promoters of stress genes such as *fbp1* (14,30). Atf1 has been shown to be involved in chromatin remodeling and gene activation in response to stresses (49–51). We therefore investigated whether mlonRNA transcription affects Atf1 binding. We blocked mlonRNA induction by treating cells with a transcription inhibitor 1,10-phenanthroline (52) immediately after glucose depletion (Figure 2A). Our previous study showed that this treatment completely abolishes the cascade expression of mlonRNAs (30), and consistent with this report, the 1,10-phenanthroline treatment attenuated Pol II accumulation at the *fbp1* locus (Supplementary Figure S1A). We then studied Atf1 occupancy at UAS1 in *fbp1* by ChIP-qPCR assays, and found that Atf1 was slightly enriched at UAS1 in glucose-rich conditions and markedly accumulated (~8-fold over background) upon glucose depletion (left panel of Figure 2B). Notably, such accumulation was dramatically reduced by the 1,10-phenanthroline treatment. We obtained similar results when cells were treated with another transcription inhibitor thiolutin (Supplementary Figure S1B–D) (53). The effect of transcription inhibition appeared to be locus-specific, because 1,10-phenanthroline and thiolutin had almost no effect on Atf1 binding at the *SPBC660.05* locus (Figure 2B and Supplementary Figure S1D) (54). We also confirmed by Western blotting that both inhibitors did not markedly reduce the amount of Atf1 (Supplementary Figure S1E).

To further rule out a possibility of secondary effects by transcription inhibitors, we constructed and analyzed a strain that cannot undergo the cascade transcription of mlonRNAs at the *fbp1* locus. This allele (*fbp1-*$P_{bc}$*Δ::spacer*) has a replacement of the region between UAS1 and UAS2, which includes transcription start sites (TSSs) for the two shorter mlonRNA species (mlonRNA-b and -c), by a sequence of equivalent length lacking any potential promoters (Figure 2C). The *fbp1-*$P_{bc}$*Δ::spacer* strain produced only longer versions of lncRNAs that were similar to mlonRNA-a and -b (Figure 2D, black and white arrowhead respectively). The positional shift of TSSs for the shortest mlonRNA-c was not successful in this *fbp1-*$P_{bc}$*Δ::spacer* allele, and *fbp1* mRNA induction was markedly delayed (Figure 2D and E). Using this *fbp1-*$P_{bc}$*Δ::spacer* strain, we examined Atf1 binding to the *fbp1* promoter. As expected, *fbp1-*$P_{bc}$*Δ::spacer* exhibited reduced Atf1 binding (Figure 2F), accompanied by delayed histone H3 eviction at UAS1 and UAS2 (Figure 2G).

These results demonstrate that the cascade transcription of mlonRNAs indeed promotes Atf1 binding at the *fbp1* promoter before mRNA induction. As the Atf1-UAS1 interaction is important for mlonRNA transcription (see Figure 1B), it is likely that the Atf1 binding and mlonRNA transcription mutually facilitate each other, building a positive feedback loop for *fbp1* transcriptional activation. The

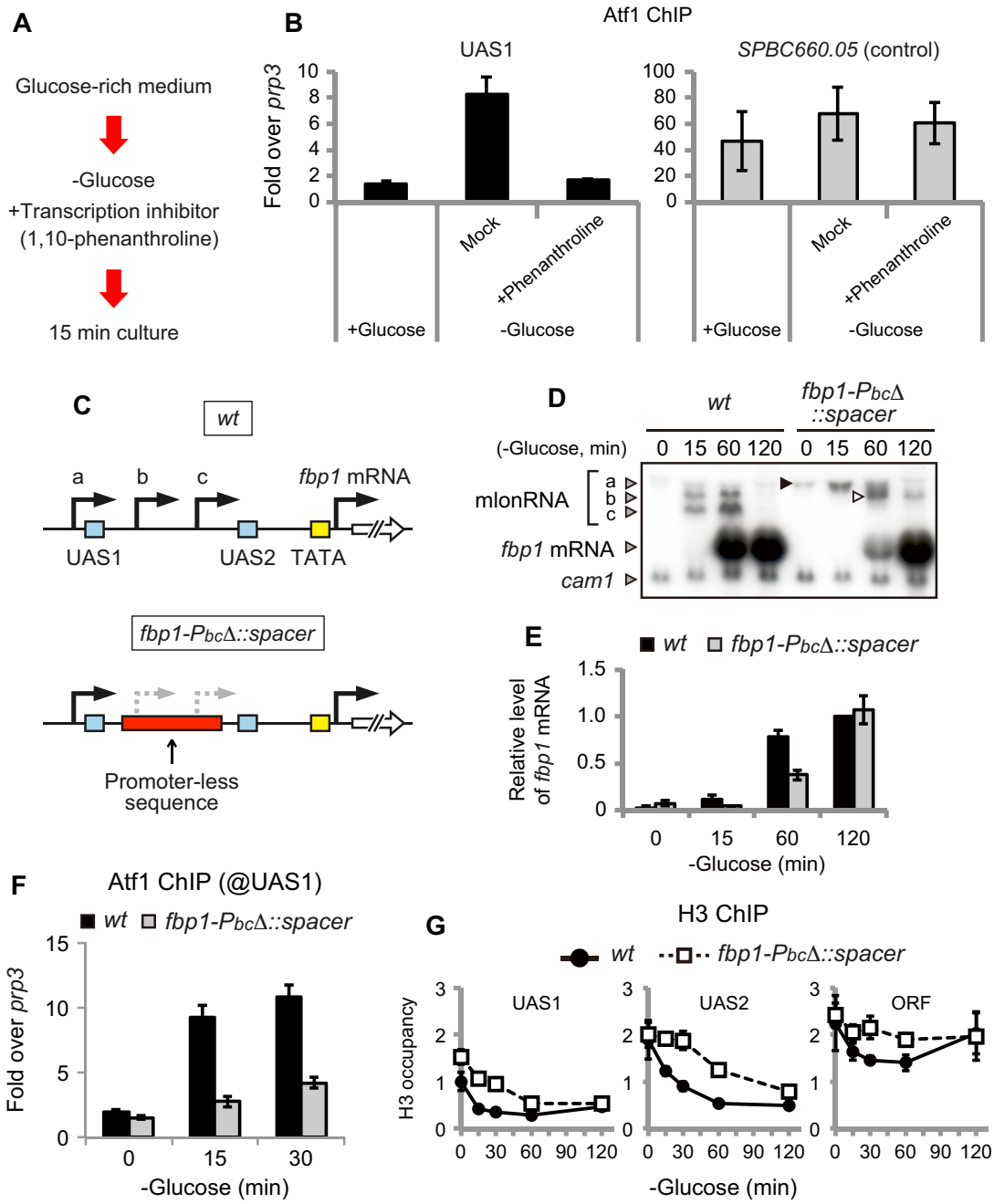


**Figure 2.** Cascade-like transcription of mlonRNAs promotes Atf1 binding to the *fbp1* promoter. (**A**) Experimental diagram of Figure 2B. Wild type cells in glucose-rich medium (+Glucose) were shifted to low-glucose medium (−Glucose). Immediately after the shift, cells were treated with 1/1000 volume of ethanol with (+Phenanthroline) or without (Mock) 1,10-phenanthroline, and cultured for 15 min. (**B**) ChIP-qPCR was performed using an anti-Atf1 antibody. The IP/WCE value for the *prp3* gene was used to define the background signal for normalization. Error bars represent standard deviations from three biological replicates. (**C**) Schematic diagram of the *fbp1-Pbc*Δ*::spacer* allele. (**D**) Northern blotting was conducted as in Figure 1B. Positions of the authentic mlonRNAs (mlonRNA-a, -b, and -c) are indicated on the left side. Black and white arrowheads indicate an mlonRNA-a-like and an mlonRNA-b-like transcript respectively. (**E**) Quantification of the Northern blotting data in Figure 2D. Relative RNA levels normalized with that of *cam1* mRNA are shown (the value of *wt* at 120 min was set to 1). Error bars represent standard deviations from three biological replicates. (**F**) ChIP-qPCR was performed as in Figure 2B. Error bars represent standard deviations from three biological replicates. (**G**) ChIP-qPCR of H3 was conducted as in Figure 1C. Error bars represent standard deviations from three biological replicates. Note that some error bars are invisibly small.

recruitment of Gcn5 is apparently not required for this loop, because loss of Gcn5 did not markedly affect mlonRNA expression or Atf1 occupancy at UAS1 (Figure 1H and Supplementary Figure S2).

### lncRNA transcription promotes Atf1 binding in *cis*

It has been reported that lncRNAs can function either in *cis* or in *trans* (3). We thus investigated whether ectopic synthesis of mlonRNAs can promote Atf1-UAS1 interaction in *trans*. In a haploid strain harboring the *fbp1-P*$_{bc}$*Δ::spacer* allele (on chromosome 2), a DNA fragment containing the entire *fbp1* sequence was introduced into the *nmt1-gut2* region (on chromosome 3) (Figure 3A). Northern blot analysis indicated that this strain expressed mlonRNA-b and -c from the inserted copy at comparable levels to those in wild type (Figure 3B). Using this strain, we conducted ChIP-qPCR assays to test whether the ectopic production of mlonRNAs restores Atf1 binding at the *fbp1-P*$_{bc}$*Δ::spacer* allele. By utilizing PCR primers illustrated in Figure 3A, we measured the specific signal from the *fbp1-P*$_{bc}$*Δ::spacer* allele. As shown in Figure 3C, the ectopic expression of mlonRNA-b and -c did not restore Atf1 binding to UAS1 at the *fbp1-P*$_{bc}$*Δ::spacer* allele. Therefore, mlonRNA transcription is unlikely to promote the Atf1 binding in *trans*, and most of its activity is carried out in *cis*.

The human lncRNA *ANRIL* (antisense noncoding RNA in the *INK4* locus) represses gene expression by serving as a '*cis*-acting tether' that connects Polycomb repressing complex 1 (PRC1) and PRC2 to its target locus, and this physical linkage can be disrupted by RNase treatment (55). In addition, *S. pombe* Atf1 can also form a complex with RNA (56). We therefore explored whether mlonRNAs also directly tether Atf1 to the *fbp1* chromatin region in *cis*. Crosslinked Atf1-chromatin complexes were first immunoprecipitated with the anti-Atf1 antibody as in the above ChIP experiment. The precipitates bound to antibody-conjugated beads were treated with RNase H or a cocktail of RNase A and $T_1$, followed by extensive washes. The remaining DNA on the beads was used for qPCR analysis. We found that both types of RNase treatment did not significantly decreased Atf1 binding at UAS1 (Supplementary Figure S3). Therefore, mlonRNAs themselves are unlikely to serve as *cis*-acting tethers.

### Roles of transcription in genome-wide Atf1 binding

To further explore the general importance of noncoding RNA transcription in Atf1 recruitment, we next performed Atf1 chromatin immunoprecipitation-sequencing (ChIP-seq) analysis. Consistent with previous genome-wide studies using microarrays (43,54), Atf1 was enriched at ∼300 genomic loci even in the absence of stress (Supplementary Figure S4A). After glucose depletion, 137 Atf1 peaks were abolished but 270 peaks newly appeared, resulting in the detection of ∼450 peaks in total (Supplementary Figure S4A). About 200 loci showed more than a two-fold increase in Atf1 occupancy in response to glucose depletion (Supplementary Figure S4B). The number of these enhanced Atf1-binding sites was apparently much larger than that observed under oxidative stress (54).

To identify transcription-dependent Atf1-binding sites, we perfomed Atf1 ChIP-seq analysis on cells treated with 1,10-phenanthroline immediately after glucose depletion. The effect of 1,10-phenanthroline on the binding profile of Atf1 was reproduced in two biological replicates (Supplementary Figure S5A). We detected 50 'transcription-enhanced Atf1-binding sites' (loci exhibiting more than a two-fold reduction in Atf1 occupancy in 1,10-phenanthroline-treated cells, Figure 4A and B). Of them, 11 loci (red dots in Figure 4B) showed an even greater fold decrease in Atf1 occupancy than *fbp1*. 52 sites conversely exhibited more than a two-fold increase in Atf1 binding in 1,10-phenanthroline-treated cells (Figure 4A and B). Atf1-binding sites that were less affected by 1,10-phenanthroline ($-1 \leq \log_2$ fold change $\leq 1$) were referred to as 'transcription-independent Atf1-binding sites' (Figure 4B).

We compared the extent of Atf1 enrichment between transcription-enhanced and -independent sites. Atf1 occupancy at transcription-enhanced sites was low in glucose-rich conditions but dramatically elevated after glucose depletion (Figure 4C and D), whereas that at transcription-independent sites was relatively high in glucose-rich conditions and less increased after glucose depletion. In addition, at a large proportion of the transcription-enhanced sites (41/50 sites), Atf1 was detectable only in low-glucose conditions (Supplementary Figure S6). These data suggest that transcription-enhanced sites exhibit greater induction of Atf1 binding than independent sites upon glucose starvation.

In comparison with the previous RNA-seq data (14), we found that transcription-enhanced Atf1-binding sites were associated with nearby transcription (Figure 4E). It should be noted that 36% of the transcription-enhanced Atf1-binding sites (18/50 sites) were located near known Atf1-target genes (Supplementary Table S3). Furthermore, expression of potential noncoding RNAs was induced from 24 transcription-enhanced sites in response to glucose depletion (Figure 4F, Supplementary Figure S7, and Supplementary Table S3). These data support that, at transcription-enhanced sites, Atf1 binding is induced by nearby transcription of Atf1-target genes or noncoding RNAs as is observed at *fbp1*.

### Transcription-enhanced Atf1-binding sites exhibit distinct chromatin features

We then studied local chromatin features surrounding transcription-enhanced and -independent sites. Histone H3 density in the previous ChIP-seq datasets (14) was plotted versus the distance from the Atf1 peaks. When glucose was abundant, transcription-enhanced Atf1-binding sites showed higher H3 density than transcription-independent ones (Figure 5A and B). After glucose depletion, H3 occupancy was decreased at transcription-enhanced sites, becoming comparable to that of transcription-independent peaks. We also performed ChIP-seq analysis for H3K9ac, and the data indicated that the marked histone reduction at transcription-enhanced Atf1 peaks was accompanied with a substantial increase in H3K9ac levels (Figure 5C and D). These chromatin features observed at transcription-

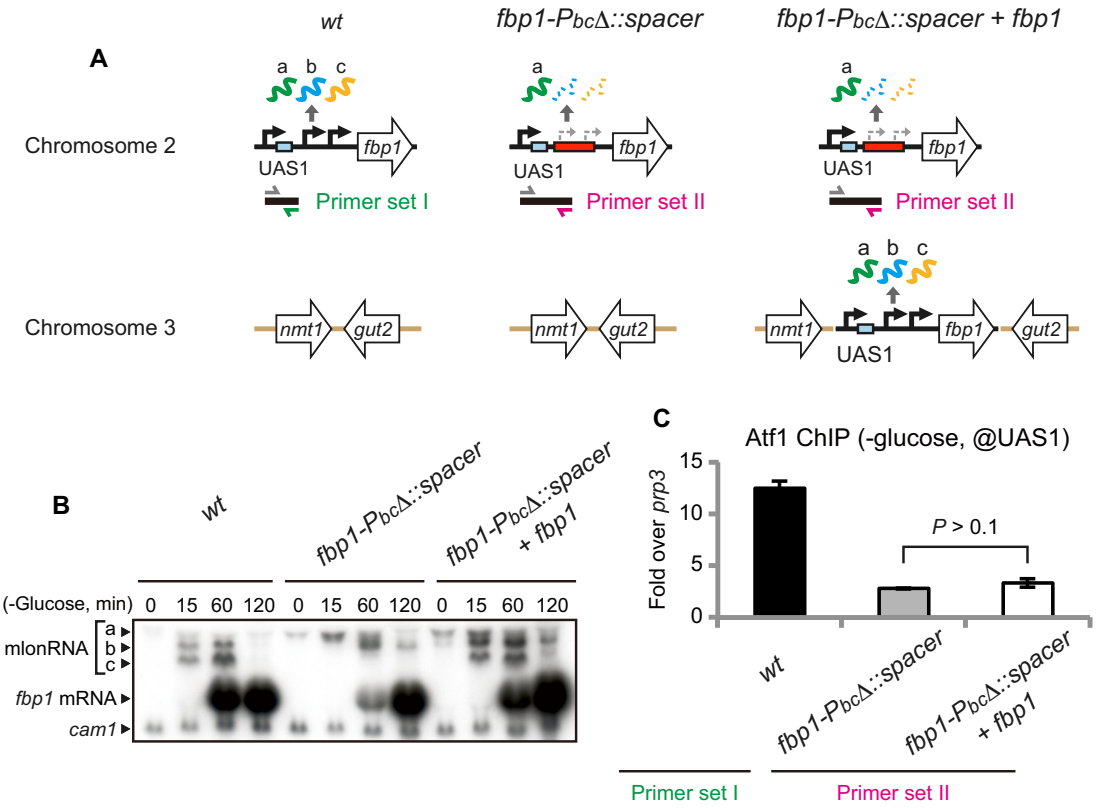


**Figure 3.** Transcription of mlonRNAs does not affect Atf1-UAS1 association in *trans*. (**A**) Schematic representation of ectopic mlonRNA expression. Primer sets used in Figure 3C are shown. (**B**) Northern blotting was performed as in Figure 1B. The image was obtained from the same film as for Figure 2D. (**C**) ChIP-qPCR was carried out as in Figure 2B using the primer sets illustrated in Figure 3A. Cells were cultured in low-glucose medium for 15 min. Error bars represent standard deviations from three biological replicates. Two-tailed *t*-test was performed to calculate *P*-value.

enhanced sites were very similar to those observed in the *fbp1* upstream segment.

### lncRNA transcription antagonizes the Tup11-Tup12 corepressors to promote Atf1 binding

To identify factors defining transcription-enhanced binding of Atf1, we focused on the Groucho/Tup1-like global corepressors Tup11 and Tup12, which redundantly repress a number of Atf1-dependent genes including *fbp1* (39,40,57,58). Tup11 and Tup12 are homologs of *S. cerevisiae* Tup1, which blocks promoter binding of the transcription factor Rap1 to control glucose starvation-induced genes (59). These findings suggest potential roles of Tup11 and Tup12 in the control of Atf1 binding.

We first examined the role of Tup11 and Tup12 in Atf1 binding to UAS1 in *fbp1*. ChIP-qPCR analysis revealed that, when glucose was abundant, a *tup11Δ tup12Δ* double deletion had only a slight effect on Atf1 binding at UAS1 (Figure 6A). However, in response to glucose depletion, *tup11Δ tup12Δ* cells greatly increased Atf1 occupancy compared to wild type. This extremely high occupancy of Atf1 is consistent with hyper-induction of *fbp1* mRNA observed in *tup11Δ tup12Δ* cells (Supplementary Figure S8) (30). Thus, in glucose-poor conditions, Tup11 and Tup12 are likely to weaken Atf1 binding at UAS1 to prevent *fbp1* overexpression.

The *fbp1-P$_{bc}$Δ::spacer* mutation, which impaired the cascade transcriptional amplification of mlonRNAs, dramatically decreased Atf1 binding at UAS1 in cells harboring wild type Tup11 and Tup12 (Figure 2D and F), indicating that the cascade transcription of mlonRNAs plays an important role in the Atf1 recruitment. We therefore hypothesized that transcription of mlonRNAs may facilitate Atf1–DNA interaction by attenuating the repressive function of Tup proteins. We tested this idea by using a *tup11Δ tup12Δ* strain carrying the *fbp1-P$_{bc}$Δ::spacer* allele. We first confirmed that this strain showed a defect in the cascade expression of mlonRNAs, although residual transcription of mlonRNA-a/b was observed as in *fbp1-P$_{bc}$Δ::spacer* cells harboring wild type Tup11 and Tup12 (Supplementary Figure S8). We also found that, in the *tup11Δ tup12Δ* background, the *fbp1-P$_{bc}$Δ::spacer* allele displayed only a negligible decrease in Atf1 occupancy (right panel of Figure 6B). Thus, the reduction of Atf1-UAS1 interaction at the *fbp1-PbcD::spacer* allele is mediated by functions of Tup11 and Tup12. This supports the notion that the transcriptional cascade of mlonRNAs can facilitate Atf1 recruitment by antagonizing Tup11 and Tup12.

We next examined the effect of 1,10-phenanthroline in *tup11Δ tup12Δ* cells (Figure 6C). In contrast to the *fbp1-P$_{bc}$Δ::spacer* mutation, 1,10-phenanthroline treatment leads to a complete transcriptional inhibition of mlonRNAs including mlonRNA-a/b (30). We found that the

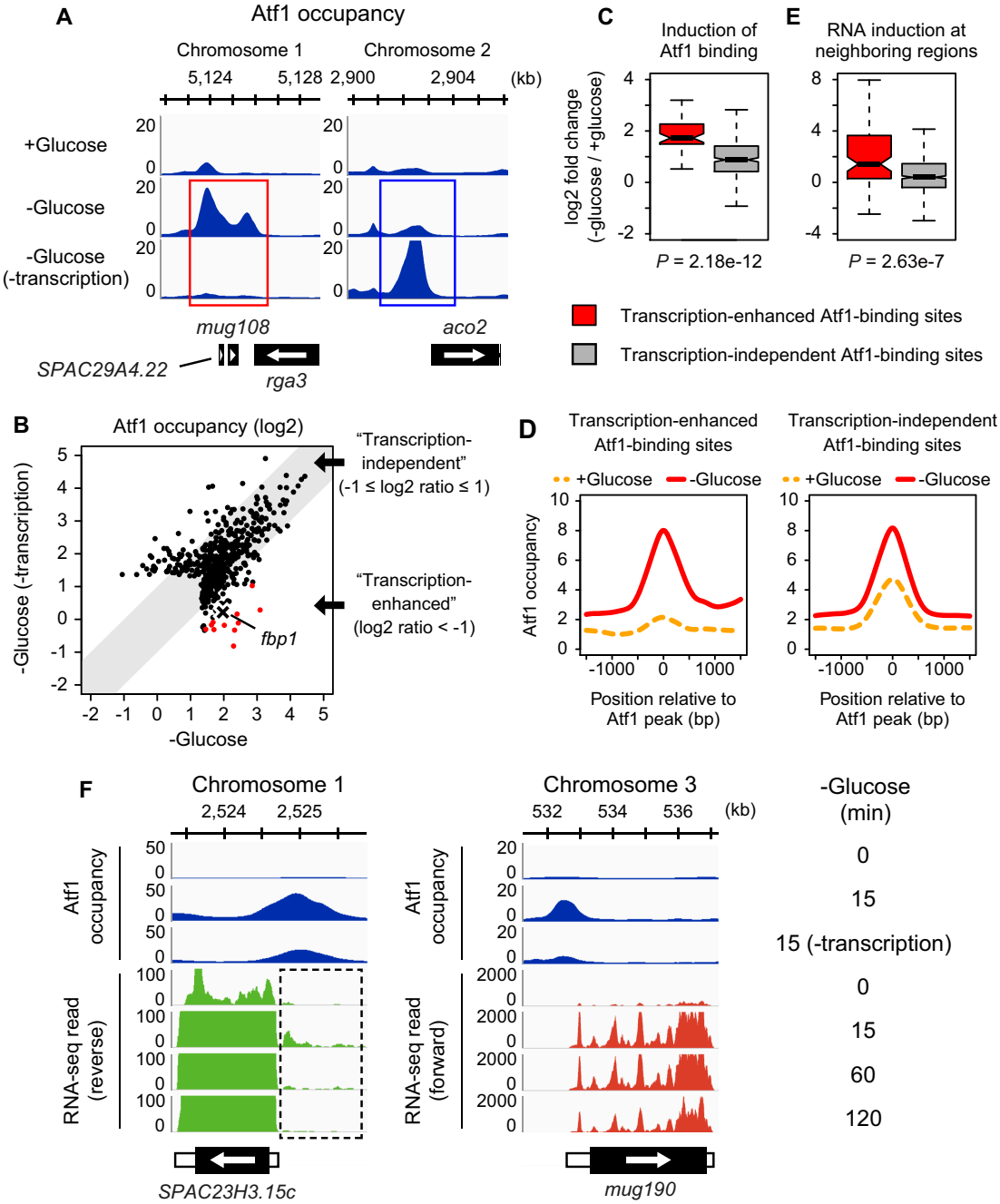


**Figure 4.** Genome-wide analysis of transcription-enhanced binding of Atf1. (**A**) ChIP-seq profile of Atf1. The data were visualized using the Integrative Genomics Viewer (78). Atf1 peaks with decreased or increased occupancy upon 1,10-phenanthroline treatment are indicated with a red rectangle and blue rectangle, respectively. ORFs are indicated with black boxes at the bottom. (**B**) Comparison of Atf1 binding in glucose-starved cells with or without 1,10-phenanthroline. The Atf1 peak regions detected in either of the two conditions (total 552 peaks) were subjected to the analysis. A black cross represents *fbp1*, and red dots represent loci that showed a greater fold decrease in Atf1 occupancy than *fbp1*. (**C** and **E**) Boxplots showing fold changes in Atf1 occupancy and RNA expression around Atf1-binding sites (outliers are not shown). The Atf1 peak regions detected in glucose-starved cells without 1,10-phenanthroline (total 461 peaks) were subjected to the analyses. Signals were compared before (+glucose) and after 15 min of glucose depletion (−glucose). Wilcoxon test was performed to calculate *P*-values. (**D**) Average profiles of Atf1 occupancy. Plots were compared before (+Glucose) and after 15 min of glucose depletion (−glucose). The Atf1 peak regions detected in glucose-starved cells without 1,10-phenanthroline were subjected to the analysis. (**F**) ChIP-seq profile of Atf1 and RNA-seq data are shown for two Atf1-target genes *SPAC23H3.15c* and *mug190* (51). ORFs (black boxes), 5′- and 3′-untranslated regions (white boxes) are indicated at the bottom. Potential noncoding RNA expression is indicated with a black dashed rectangle.

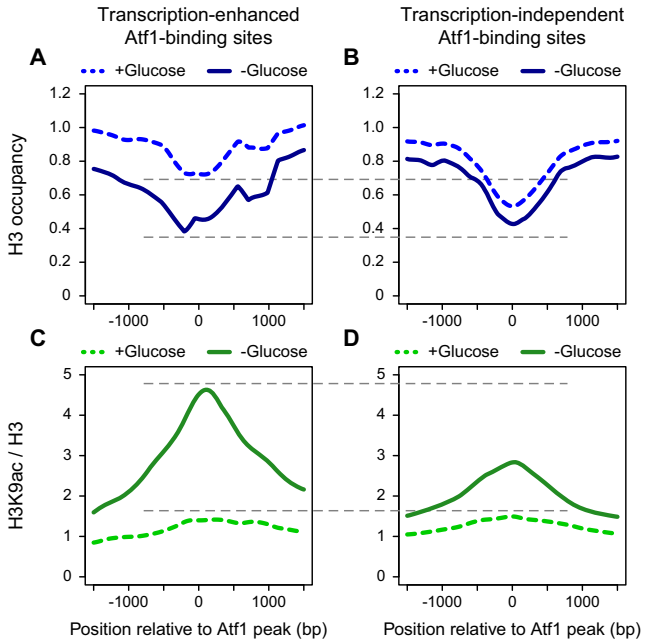


**Figure 5.** Transcription-enhanced Atf1-binding sites exhibit distinct chromatin features compared to transcription-independent sites. Average profiles of H3 occupancy (**A** and **B**) and H3K9ac/H3 (**C** and **D**) around Atf1-binding sites are shown. The Atf1 peak regions detected in glucose-starved cells without 1,10-phenanthroline were subjected to the analysis. Plots were compared before (+glucose) and after 15 min in low-glucose medium (−glucose). Gray dashed lines are shown for comparison.

complete absence of mlonRNA transcription severely repressed Atf1 binding to UAS1 even in the absence of Tup11 and Tup12.

Taken together, these results suggest the presence of Tup-dependent and -independent transcription-coupled mechanisms for the recruitment of Atf1 to UAS1. We postulate that 1,10-phenanthroline (completely abolishing the transcriptional cascade of mlonRNAs) inhibits both mechanisms, but the *fbp1-P*$_{bc}$*Δ* mutation (allowing residual transcription of mlonRNA-a/b) mainly affects the Tup-dependent one.

### Genome-wide analysis of antagonistic regulation by lncRNAs and Tup11–Tup12

To explore the antagonistic action between upstream lncRNA transcription and Tup11–Tup12 on a genome-wide scale, we performed Atf1 ChIP-seq analysis using *tup11Δ tup12Δ* cells during glucose starvation. The *tup11Δ tup12Δ* double deletion increased Atf1 occupancy more than two-fold at 234 sites (Supplementary Table S4), and 76 loci (red dots in Figure 6D) showed a greater fold increase in Atf1 occupancy than *fbp1*. In addition, these changes were highly reproducible (Supplementary Figure S5B).

By analyzing the effects of transcription inhibition and of *tup11Δ tup12Δ* on Atf1 occupancy, we next determined potential target sites for the antagonistic control by RNA transcription and Tup proteins. We selected Atf1 peaks with more than two-fold increase in Atf1 occupancy in *tup11Δ tup12Δ* cells (Figure 6D, 'Tup-repressed binding sites'). Among the 461 Atf1 peaks detected in glucose-starved wild type cells, 71 sites including *fbp1* were placed into this group (Figure 6E). Of these, 14 sites were classified as transcription-enhanced Atf1-binding sites, and this overlap was statistically significant. These potential common target sites shared four other features in glucose-poor conditions: strong induction of Atf1 binding, presence of nearby transcription, nucleosome eviction, and high H3K9 acetylation (Supplementary Figure S9).

Notably, among the 14 Atf1-binding sites that underwent the antagonistic regulation by transcription and Tup11-Tup12, six sites were located upstream of genes that are involved in adaptation to low glucose conditions. These genes include *fbp1*, the hexose transporters *ght1*, *ght4*, *ght5* and *ght8* (60,61), and the transcription factor *rsv1* (essential for cellular survival during stationary phase (62)) (Figure 6F, Supplementary Figures S10 and S11). As is observed at *fbp1* (14,30), potential noncoding RNAs were transcribed from the upstream segments of *ght1*, *ght5*, and *rsv1* near Atf1 peaks (Figure 6F, Supplementary Figure S11A and B, indicated with dashed rectangles). The Atf1-binding sites at the *ght4* and *ght8* loci were seemingly not associated with noncoding RNA transcription (Figure 6F and Supplementary Figure S11C). However, we previously showed that the *ght4* gene produces a couple of upstream transcripts different from the mRNA in length (14), which are reminiscent of mlonRNAs. In addition, judging from our previous RNA-seq dataset (14), the *ght8* locus apparently has at least two TSSs (Supplementary Figure S11C), implying that the gene also produces multiple kinds of transcripts.

### Physical interaction between upstream transcripts and Tup11-Tup12

Some lncRNAs bind to their target proteins to inhibit their functions (3). We therefore examined physical interactions between upstream transcripts and Tup proteins. RNA immunoprecipitation assays were performed using strains expressing Flag-tagged Tup11 or Tup12 from its endogenous locus. RNA co-purified with these proteins was reverse transcribed and quantified by real-time PCR. Since mlonRNA-a, -b, and -c overlap each other and are difficult to discriminate, we quantified the sum of these mlonRNA species using the primer pair illustrated in Figure 7A. mlonRNAs were highly enriched in the Tup11-Flag and Tup12-Flag precipitates compared to that from an untagged control strain (Figure 7B), indicating that mlonRNAs indeed bind to Tup11 and Tup12 in *vivo*. We also performed RNA immunoprecipitation assays using primers for other loci illustrated in Figure 6F, and found that Tup proteins physically interacted with potential upstream transcripts of *ght1* and *ght4* loci (Figure 7C). These RNAs likely antagonize Tup11 and Tup12 by physical interactions and thus promote Atf1 binding at the sites of transcription.

## DISCUSSION

Our study demonstrates that upstream lncRNA transcription plays key roles in regulating transcription factor binding. Three major findings can be summarized as follows: (i) in response to glucose starvation, transcription of upstream lncRNAs promotes binding of the transcription factor Atf1

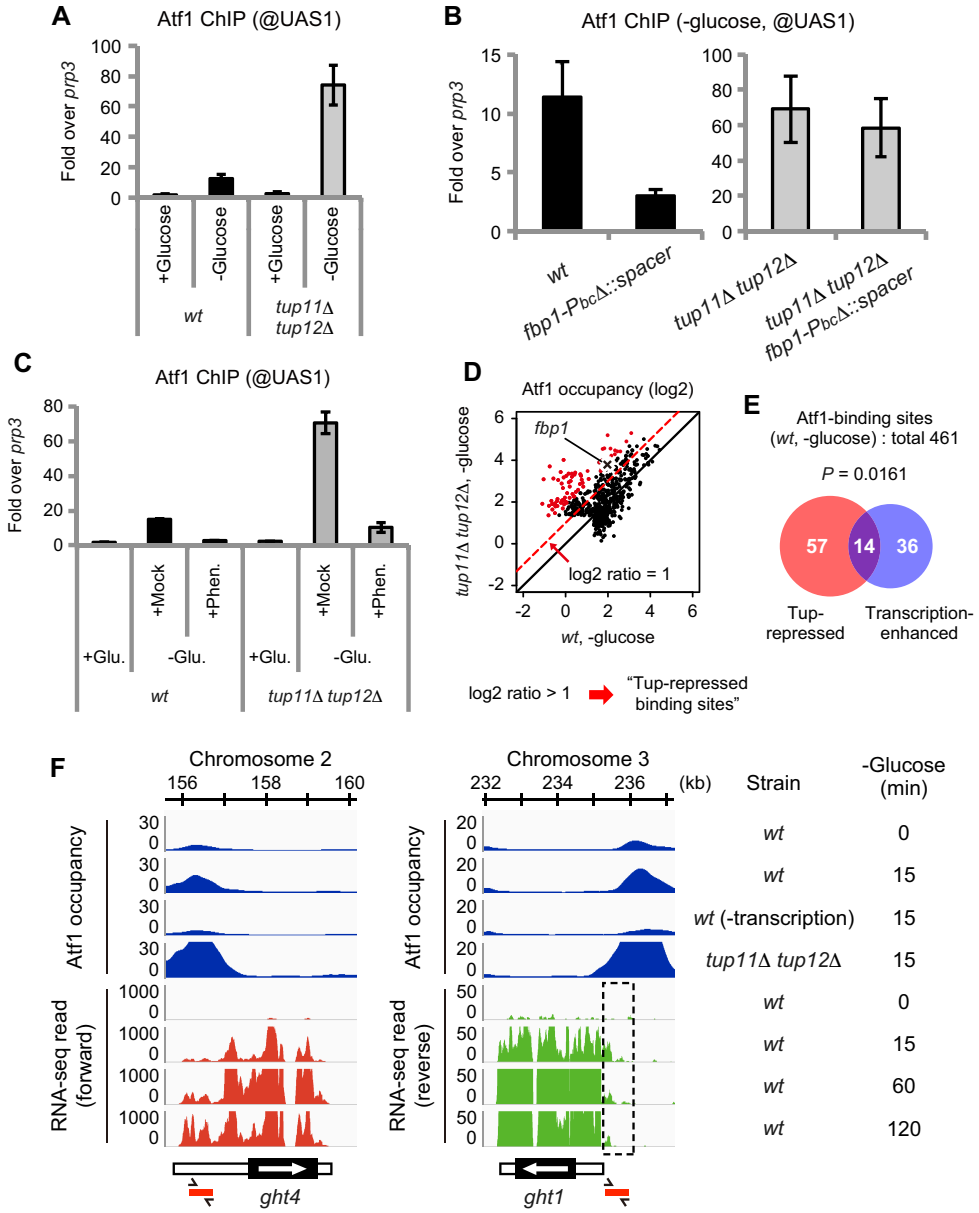


**Figure 6.** Transcription and Tup11-Tup12 antagonistically modulate Atf1 binding at a subset of genes. (**A**) ChIP-qPCR was conducted as in Figure 2B. Cells were collected before (+glucose) and after (−glucose) 15 min of culture in low-glucose medium. Error bars represent standard deviations from four biological replicates. (**B**) The effect of *fbp1-P*$_{bc}$*Δ::spacer* on Atf1-UAS1 association was examined in the presence (left panel) or absence of Tup11 and Tup12 (right panel). Cells were cultured in low-glucose medium for 15 min. Error bars represent standard deviations from three biological replicates. (**C**) Cell culture and ChIP-qPCR was performed as in Figure 2B. Error bars represent standard deviations from two biological replicates. (**D**) Comparison of Atf1 binding in glucose-starved wild type and *tup11Δ tup12Δ* cells. The Atf1 peaks detected in either of the two strains (total 624 sites) were subjected to the analysis. A black cross represents *fbp1*, and red dots represents loci that showed a greater fold increase in Atf1 occupancy than *fbp1*. (**E**) Venn diagram showing the overlap between Tup-repressed and transcription-enhanced Atf1-binding sites. Chi-square test was performed to calculate *P*-value. (**F**) ChIP-seq profile of Atf1 and RNA-seq data are shown for two hexose-transporter genes *ght4* and *ght1*. Potential noncoding RNA expression is indicated with a black dashed rectangle. PCR fragments used for RNA immunoprecipitation in Figure 7C are indicated with red boxes.

to the *fbp1* promoter, and similar regulation is observed at other ∼50 genomic region, (ii) some upstream lncRNAs bind to the transcriptional corepressors Tup11 and Tup12, and (iii) transcription of these lncRNAs can antagonize the repressive effect of Tup11–Tup12 on Atf1 binding. We propose that chromatin recruitment of Atf1 for activation of some stress genes is enhanced by nearby transcription (Figure 8), which in many cases is of upstream lncRNA (Figures 4 and 6).

## Roles of transcription in enhanced binding of transcriptional activators

Blocking the cascade transcription of *fbp1* lncRNAs markedly impairs Atf1 binding to UAS1 (a sequence that includes an Atf1-binding site) (Figure 2F). In addition, treatment with the transcription inhibitor 1,10-phenanthroline

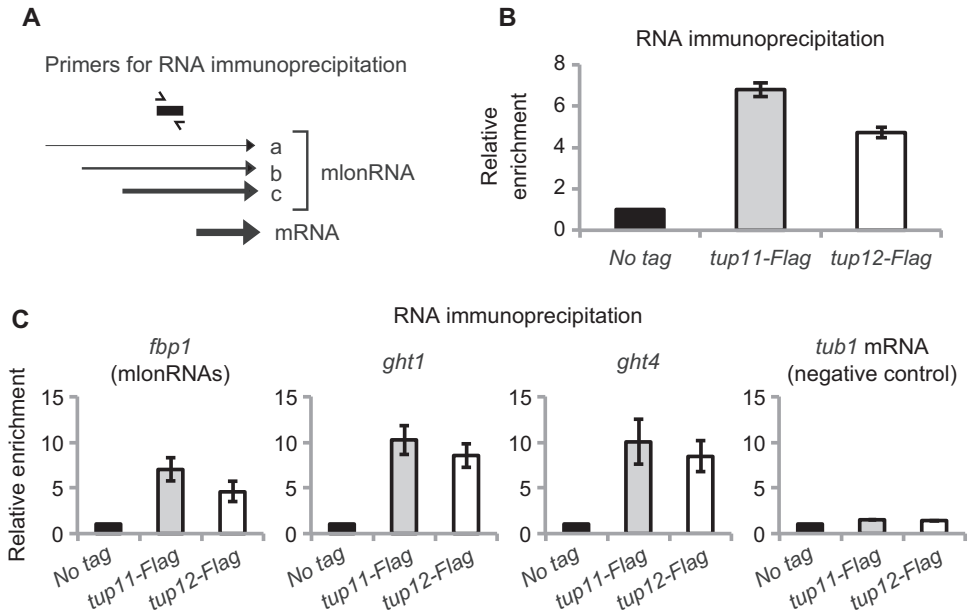


**Figure 7.** Upstream transcripts physically interact with Tup11 and Tup12. (**A**) The primer pair used for the quantification of mlonRNA in Figure 7B. (**B**) RNA immunoprecipitation with an anti-Flag antibody was carried out using untagged (*no tag*), *tup11-Flag*, and *tup12-Flag* strains cultured in low-glucose medium for 15 min. Signal ratios of total mlonRNA to *act1* mRNA were normalized to that in the untagged strain. Error bars represent standard deviations from three biological replicates. (**C**) RNA immunoprecipitation was carried out as in Figure 7B. Error bars represent standard deviations from two biological replicates.

strongly inhibits Atf1 binding at a number of target sites (Figure 4). At these sites, induction of Atf1 binding is associated with nearby transcription. These results suggest that nearby transcription can locally facilitate DNA binding of Atf1 at least in some chromosomal locations. In addition, Atf1 binding is also required for *fbp1* lncRNA expression (Figure 1B), and transcription-induced binding of Atf1 often occurs near known Atf1-target genes (Figure 4F and Supplementary Table S3). Altogether, it is likely that Atf1 binding to target sites and the nearby transcription mutually promote each other, comprising a positive feedback gene regulation circuit.

What are the advantages of the transcription-dependent regulation of Atf1 binding? Positive feedback mechanisms enable 'switch-like' sharp and continuous activation of target genes in response to stimuli (63). Thus, self-reinforcing binding of Atf1 via nearby transcription likely contributes to kinetic control of gene induction as is observed at *fbp1* (Figure 2E), to ensure appropriate gene expression responses to lethal stresses. In addition, the transcription-based mechanism, which do not require protein synthesis, is supposed to be beneficial during the very beginning phase of stress adaptation, in which cells globally repress translation (31,64,65).

### Mechanisms of the transcription-enhanced binding of Atf1

The molecular mechanisms underlying *fbp1* transcriptional activation provide important clues to understanding how lncRNA transcription regulates Atf1 binding. Here we suggest two types of lncRNA transcription-coupled mechanisms: Tup-dependent and -independent pathways (Figure 8).

In the Tup-dependent pathway, upstream transcripts modulate functions of the global corepressors Tup11 and Tup12, homologs of *Drosophila* Groucho and *S. cerevisiae* Tup1 (66). Tup11 and Tup12 inhibit Atf1 binding at a number of target sites, and this effect can be antagonized by upstream lncRNA transcription (Figure 6). Moreover, RNA immunoprecipitation assays revealed that Tup11 and Tup12 are co-purified with upstream transcripts (Figure 7). These results lead us to propose that, through physical interactions, upstream transcripts can locally attenuate inhibitory functions of Tup11 and Tup12 on Atf1 binding (Figure 8A). Given the *cis* effect of *fbp1* upstream lncRNA (Figure 3), nascent transcripts appear to antagonize Tup11 and Tup12 at the sites of upstream transcription. Such a lncRNA-based local modulation mechanism may be important for gene-specific activation of transcription, because Tup proteins repress a large number of stress genes (70) but their effects need to be alleviated only at a subset of genes in response to a particular stimulus (33,57).

*S. cerevisiae* Tup1 regulates nucleosome positioning at target promoters (67–69), and impedes DNA binding of the transcription factor Rap1 through the chromatin remodeler Isw2 and the histone deacetylase Hda1 (59). We previously reported that chromatin alteration at *fbp1* is tightly repressed by Tup11 and Tup12 (33,37,58). Thus, in the Tup-dependent model, we postulate that Atf1 binding is repressed by Tup-mediated chromatin repression, and loci with upstream transcription evade this repression under stress conditions.

The data in this study also suggest that a Tup-independent mechanism is involved in lncRNA transcription-coupled binding of Atf1. When we treated *tup11Δ tup12Δ* cells with 1,10-phenanthroline, Atf1-UAS1

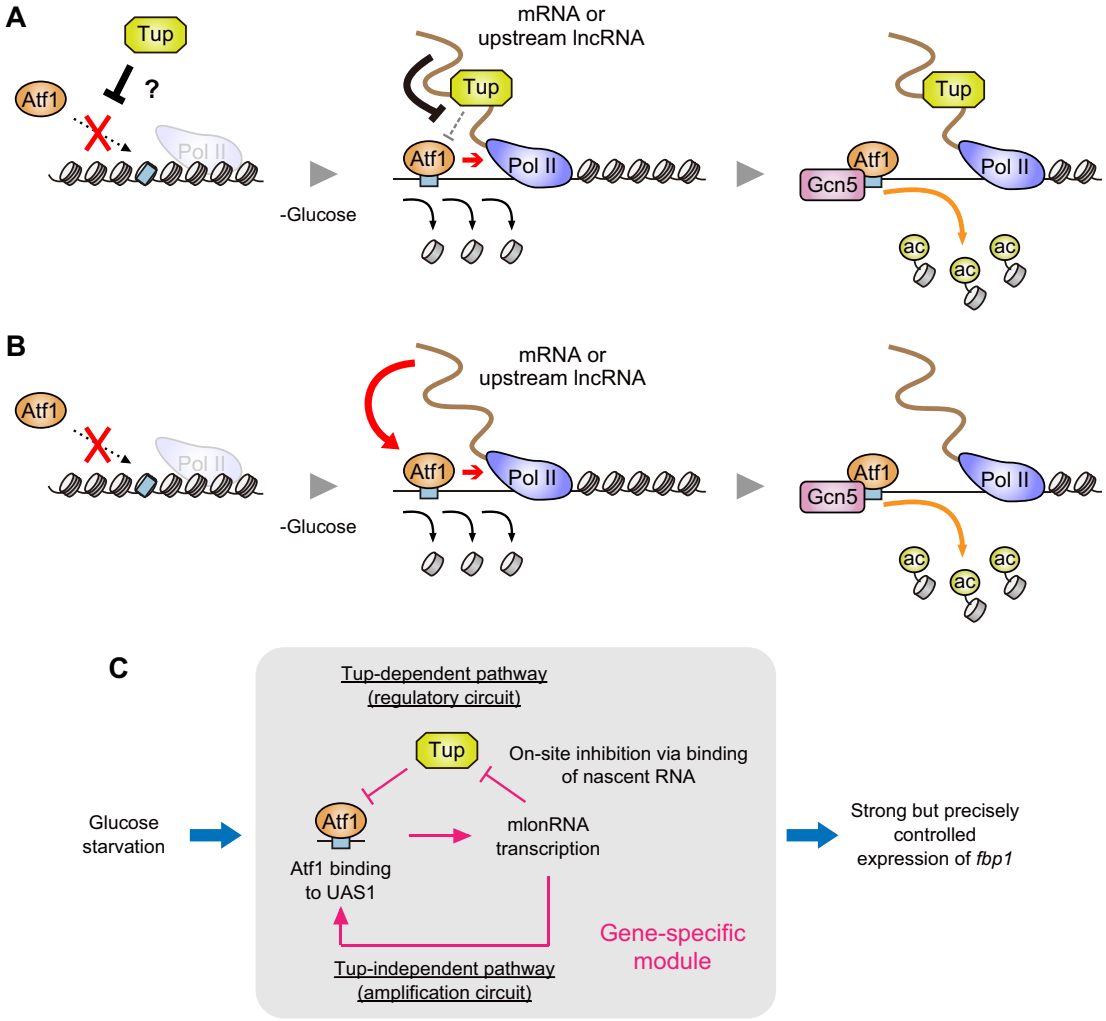


**Figure 8.** Models for transcription-mediated regulation of Atf1 binding. (**A**) In glucose-rich conditions, nucleosomes occupy Atf1-binding sites and thus Atf1 cannot associate with them efficiently. Tup11 and Tup12 may also repress Atf1 binding in glucose-rich conditions. Glucose starvation induces transcription at nearby regions (coding and noncoding regions are both possible). This transcription locally antagonizes the inhibitory effect of Tup11-Tup12 on Atf1 binding, possibly through physical interactions between Tup proteins and nascent transcripts. Atf1 binding further activates neighboring transcription to form positive feedback loops, and Atf1 recruits Gcn5 to induce histone acetylation and chromatin disassembly. (**B**) Transcription can also promote Atf1 binding independently of Tup proteins, possibly by enhancing DNA accessibility at Atf1-binding sites (e.g. Pol II-dependent chromatin remodeling). (**C**) The overall flow of *fbp1* regulation. Upon glucose starvation, mlonRNA transcription promotes Atf1-UAS1 association through Tup-dependent and -independent pathways. In the Tup-dependent pathway, mlonRNA transcription locally antagonizes Tup11 and Tup12 as described in Figure 8A, thereby allowing gene-specific activation. The Tup-independent mechanism is more directly mediated by mlonRNA transcription, possibly regulating local chromatin structure (see above). The combination of positive (the two transcription-coupled mechanisms) and negative (Tup11–Tup12) regulators of Atf1 binding enables strong but precisely regulated induction of *fbp1* expression.

interaction was severely impaired as compared to that in the mock control (Figure 6C). This clearly demonstrates that transcription can promote Atf1 binding even in the absence of Tup11 and Tup12 (Figure 8B and C).

Then, how does lncRNA transcription facilitate Atf1 binding independently of Tup proteins? In the promoter region of *fbp1*, upstream lncRNA transcription directly or indirectly promotes histone removal upon glucose depletion (Figure 2G). Similarly, transcription-enhanced Atf1-binding sites are associated with stress-induced histone eviction (Figure 5A). It is therefore plausible that the increase in DNA accessibility after local histone eviction promotes the Atf1 binding in regions for the upstream noncoding RNA transcription (Figure 8B). Pol II may play roles in enhancing DNA accessibility, as is reported in previous studies (71,72). Once the DNA regions become accessible, Atf1 binding itself or the subsequent recruitment of Gcn5 likely contributes to further chromatin opening (Figures 1 and 8B) (50,73,74), enabling the dramatic histone eviction observed at transcription-enhanced sites (Figure 5A).

About the regulatory mechanism of *fbp1* expression, we propose a model described in Figure 8C. In this model, Atf1 binding is promoted by the two transcription-coupled mechanisms discussed above. Tup11 and Tup12 antagonize the positive feedback circuit for Atf1-UAS1 interaction enhanced by lncRNA transcription. These mechanisms likely comprise a gene-specific regulatory module that enables strong but precisely controlled expression of *fbp1*.

### Role of RNAs transcribed from gene regulatory elements

The data in this study suggest potential roles for upstream noncoding transcription in choreographing actions of transcriptional regulator proteins in eukaryotes. Notably, genome-wide studies have shown that metazoan enhancers are also associated with noncoding RNAs (75). In addition, a recent study on murine embryonic stem cells has suggested that RNAs that originate from gene regulatory elements (promoters and enhancers) facilitate trapping of the transcription factor YY1 at the sites of their transcription (76). Thus, the molecular mechanism proposed here may be conserved in diverse eukaryotes. Further investigations on the roles of RNA transcription at regulatory DNA regions will provide important clues to understand the molecular basis of enhancer functions.

## SUPPLEMENTARY DATA

Supplementary Data are available at NAR Online.

## ACKNOWLEDGEMENTS

We would like to thank Drs Takashi Sutani and Ryuichiro Nakato for advice on the usage of DROMPA, and Sachiko Mura for technical support with ChIP-seq experiments. Dr Sutani also gave us useful recommendations on the usage of thiolutin. We thank Ohta laboratory members for helpful discussion.

## FUNDING

Japanese Society for the Promotion of Science Fellows [13J08245 to N.T., 12J02844 to A.O., 3114003, 21241046, 26291018 to K.O.]; Scientific Research on Innovative Areas [221S0002 to Y.S. and S.S.]; Platform for Dynamic Approaches to Living System from the Ministry of Education, Culture, Sports, Science and Technology, Japan. Funding for open access charge: Japanese Society for the Promotion of Science.
*Conflict of interest statement.* None declared.

## REFERENCES

1. Djebali,S., Davis,C.A., Merkel,A., Dobin,A., Lassmann,T., Mortazavi,A., Tanzer,A., Lagarde,J., Lin,W., Schlesinger,F. *et al.* (2012) Landscape of transcription in human cells. *Nature*, **489**, 101–108.
2. Rhind,N., Chen,Z., Yassour,M., Thompson,D.A., Haas,B.J., Habib,N., Wapinski,I., Roy,S., Lin,M.F., Heiman,D.I. *et al.* (2011) Comparative functional genomics of the fission yeasts. *Science*, **332**, 930–936.
3. Bonasio,R. and Shiekhattar,R. (2014) Regulation of transcription by long noncoding RNAs. *Annu. Rev. Genet.*, **48**, 433–455.
4. Lee,J.T. and Bartolomei,M.S. (2013) X-inactivation, imprinting, and long noncoding RNAs in health and disease. *Cell*, **152**, 1308–1323.
5. Zhao,J., Ohsumi,T.K., Kung,J.T., Ogawa,Y., Grau,D.J., Sarma,K., Song,J.J., Kingston,R.E., Borowsky,M. and Lee,J.T. (2010) Genome-wide identification of polycomb-associated RNAs by RIP-seq. *Mol. Cell*, **40**, 939–953.
6. Khalil,A.M., Guttman,M., Huarte,M., Garber,M., Raj,A., Rivea Morales,D., Thomas,K., Presser,A., Bernstein,B.E., van Oudenaarden,A. *et al.* (2009) Many human large intergenic noncoding RNAs associate with chromatin-modifying complexes and affect gene expression. *Proc. Natl. Acad. Sci. U.S.A.*, **106**, 11667–11672.
7. Davidovich,C., Wang,X., Cifuentes-rojas,C., Goodrich,K.J., Gooding,A.R., Lee,J.T. and Cech,T.R. (2015) Toward a consensus on the binding specificity and promiscuity of PRC2 for RNA. *Mol. Cell*, **57**, 552–558.
8. Ard,R., Tong,P. and Allshire,R.C. (2014) Long non-coding RNA-mediated transcriptional interference of a permease gene confers drug tolerance in fission yeast. *Nat. Commun.*, **5**, 5576.
9. Houseley,J., Rubbi,L., Grunstein,M., Tollervey,D. and Vogelauer,M. (2008) A ncRNA modulates histone modification and mRNA induction in the yeast *GAL* gene cluster. *Mol. Cell*, **32**, 685–695.
10. Kim,T., Xu,Z., Clauder-Münster,S., Steinmetz,L.M. and Buratowski,S. (2012) Set3 HDAC mediates effects of overlapping noncoding transcription on gene induction kinetics. *Cell*, **150**, 1158–1169.
11. Van Werven,F.J., Neuert,G., Hendrick,N., Lardenois,A., Buratowski,S., Van Oudenaarden,A., Primig,M. and Amon,A. (2012) Transcription of two long noncoding RNAs mediates mating-type control of gametogenesis in budding yeast. *Cell*, **150**, 1170–1181.
12. Pinskaya,M., Gourvennec,S. and Morillon,A. (2009) H3 lysine 4 di- and tri-methylation deposited by cryptic transcription attenuates promoter activation. *EMBO J.*, **28**, 1697–1707.
13. Neil,H., Malabat,C., d'Aubenton-Carafa,Y., Xu,Z., Steinmetz,L.M. and Jacquier,A. (2009) Widespread bidirectional promoters are the major source of cryptic transcripts in yeast. *Nature*, **457**, 1038–1042.
14. Oda,A., Takemata,N., Hirata,Y., Miyoshi,T., Suzuki,Y., Sugano,S. and Ohta,K. (2015) Dynamic transition of transcription and chromatin landscape during fission yeast adaptation to glucose starvation. *Genes Cells*, **20**, 392–407.
15. Xu,Z., Wei,W., Gagneur,J., Perocchi,F., Clauder-Münster,S., Camblong,J., Guffanti,E., Stutz,F., Huber,W. and Steinmetz,L.M. (2009) Bidirectional promoters generate pervasive transcription in yeast. *Nature*, **457**, 1033–1037.
16. Seila,A.C., Calabrese,J.M., Levine,S.S., Yeo,G.W., Rahl,P.B., Flynn,R.A, Young,R. a and Sharp,P.A. (2008) Divergent transcription from active promoters. *Science*, **322**, 1849–1851.
17. Core,L.J., Waterfall,J.J. and Lis,J.T. (2008) Nascent RNA sequencing reveals widespread pausing and divergent initiation at human promoters. *Science*, **322**, 1845–1848.
18. Marquardt,S., Escalante-Chong,R., Pho,N., Wang,J., Churchman,L.S., Springer,M. and Buratowski,S. (2014) A chromatin-based mechanism for limiting divergent noncoding transcription. *Cell*, **157**, 1712–1723.
19. Schulz,D., Schwalb,B., Kiesel,A., Baejen,C., Torkler,P., Gagneur,J., Soeding,J. and Cramer,P. (2013) Transcriptome surveillance by selective termination of noncoding RNA synthesis. *Cell*, **155**, 1075–1087.
20. Wyers,F., Rougemaille,M., Badis,G., Rousselle,J.C., Dufour,M.E., Boulay,J., Régnault,B., Devaux,F., Namane,A., Séraphin,B. *et al.* (2005) Cryptic Pol II transcripts are degraded by a nuclear quality control pathway involving a new poly(A) polymerase. *Cell*, **121**, 725–737.
21. Preker,P., Nielsen,J., Kammler,S., Lykke-Andersen,S., Christensen,M.S., Mapendano,C.K., Schierup,M.H. and Jensen,T.H. (2008) RNA exosome depletion reveals transcription upstream of active human promoters. *Science*, **322**, 1851–1854.
22. Tan-Wong,S.M., Zaugg,J.B., Camblong,J., Xu,Z., Zhang,D.W., Mischo,H.E., Ansari,A.Z., Luscombe,N.M., Steinmetz,L.M. and Proudfoot,N.J. (2012) Gene loops enhance transcriptional directionality. *Science*, **338**, 671–675.
23. Wang,X., Arai,S., Song,X., Reichart,D., Du,K., Pascual,G., Tempst,P., Rosenfeld,M.G., Glass,C.K. and Kurokawa,R. (2008) Induced ncRNAs allosterically modify RNA-binding proteins *in cis* to inhibit transcription. *Nature*, **454**, 126–130.
24. Hainer,S.J., Pruneski,J.A., Mitchell,R.D., Monteverde,R.M. and Martens,J.A. (2011) Intergenic transcription causes repression by directing nucleosome assembly. *Genes Dev.*, **25**, 29–40.
25. Shah,S., Wittmann,S., Kilchert,C. and Vasiljeva,L. (2014) lncRNA recruits RNAi and the exosome to dynamically regulate *pho1* expression in response to phosphate levels in fission yeast. *Genes Dev.*, **28**, 231–244.
26. Lee,N.N., Chalamcharla,V.R., Reyes-Turcu,F., Mehta,S., Zofall,M., Balachandran,V., Dhakshnamoorthy,J., Taneja,N., Yamanaka,S., Zhou,M. *et al.* (2013) Mtr4-like protein coordinates nuclear RNA

processing for heterochromatin assembly and for telomere maintenance. *Cell*, **155**, 1–14.
27. Di Ruscio,A., Ebralidze,A.K., Benoukraf,T., Amabile,G., Goff,L.A., Terragni,J., Figueroa,M.E., De Figueiredo Pontes,L.L., Alberich-Jorda,M., Zhang,P. *et al.* (2013) DNMT1-interacting RNAs block gene-specific DNA methylation. *Nature*, **503**, 371–376.
28. Martens,J.A., Laprade,L. and Winston,F. (2004) Intergenic transcription is required to repress the *Saccharomyces cerevisiae SER3* gene. *Nature*, **429**, 571–574.
29. Hoffman,C.S. and Winston,F. (1991) Glucose repression of transcription of the *Schizosaccharomyces pombe fbp1* gene occurs by a cAMP signaling pathway. *Genes Dev.*, **5**, 561–571.
30. Hirota,K., Miyoshi,T., Kugou,K., Hoffman,C.S., Shibata,T. and Ohta,K. (2008) Stepwise chromatin remodelling by a cascade of transcription initiation of non-coding RNAs. *Nature*, **456**, 130–134.
31. Galipon,J., Miki,A., Oda,A., Inada,T. and Ohta,K. (2013) Stress-induced lncRNAs evade nuclear degradation and enter the translational machinery. *Genes Cells*, **18**, 353–368.
32. Neely,L.A. and Hoffman,C.S. (2000) Protein kinase A and mitogen-activated protein kinase pathways antagonistically regulate fission yeast *fbp1* transcription by employing different modes of action at two upstream activation sites. *Mol. Cell. Biol.*, **20**, 6426–6434.
33. Hirota,K., Hasemi,T., Yamada,T., Mizuno,K.I., Hoffman,C.S., Shibata,T. and Ohta,K. (2004) Fission yeast global repressors regulate the specificity of chromatin alteration in response to distinct environmental stresses. *Nucleic Acids Res.*, **32**, 855–862.
34. Wilkinson,M.G., Samuels,M., Takeda,T., Mark Toone,W., Shieh,J.C., Toda,T., Millar,J.B.A. and Jones,N. (1996) The Atf1 transcription factor is a target for the Sty1 stress-activated MAP kinase pathway in fission yeast. *Genes Dev.*, **10**, 2289–2301.
35. Shiozaki,K. and Russell,P. (1996) Conjugation, meiosis, and the osmotic stress response are regulated by Spc1 kinase through Atf1 transcription factor in fission yeast. *Genes Dev.*, **10**, 2276–2288.
36. Higuchi,T., Watanabe,Y. and Yamamoto,M. (2002) Protein kinase A regulates sexual development and gluconeogenesis through phosphorylation of the Zn finger transcriptional activator Rst2p in fission yeast. *Mol. Cell. Biol.*, **22**, 1–11.
37. Hirota,K., Hoffman,C.S. and Ohta,K. (2006) Reciprocal nuclear shuttling of two antagonizing Zn finger proteins modulates Tup family corepressor function to repress chromatin remodeling. *Eukaryot. Cell*, **5**, 1980–1989.
38. Asada,R., Takemata,N., Hoffman,C.S., Ohta,K. and Hirota,K. (2015) Antagonistic controls of chromatin and mRNA start site selection by Tup family corepressors and the CCAAT-binding factor. *Mol. Cell. Biol.*, **35**, 847–855.
39. Janoo,R.T.K., Neely,L.A., Braun,B.R., Whitehall,S.K. and Hoffman,C.S. (2001) Transcriptional regulators of the *Schizosaccharomyces pombe fbp1* gene include two redundant Tup1p-like corepressors and the CCAAT binding factor activation complex. *Genetics*, **157**, 1205–1215.
40. Mukai,Y., Matsuo,E., Roth,S.Y. and Harashima,S. (1999) Conservation of histone binding and transcriptional repressor functions in a *Schizosaccharomyces pombe* Tup1p homolog. *Mol. Cell. Biol.*, **19**, 8461–8468.
41. Ito,M., Kugou,K., Fawcett,J. a., Mura,S., Ikeda,S., Innan,H. and Ohta,K. (2014) Meiotic recombination cold spots in chromosomal cohesion sites. *Genes Cells*, **19**, 359–373.
42. Nakato,R., Itoh,T. and Shirahige,K. (2013) DROMPA: Easy-to-handle peak calling and visualization software for the computational analysis and validation of ChIP-seq data. *Genes Cells*, **18**, 589–601.
43. Lorenz,D.R., Meyer,L.F., Grady,P.J.R., Meyer,M.M. and Cam,H.P. (2014) Heterochromatin assembly and transcriptome repression by Set1 in coordination with a class II histone deacetylase. *Elife*, **3**, e04506.
44. Salmon-Divon,M., Dvinge,H., Tammoja,K. and Bertone,P. (2010) PeakAnalyzer: genome-wide annotation of chromatin binding and modification loci. *BMC Bioinformatics*, **11**, 415.
45. Zhu,L.J., Gazin,C., Lawson,N.D., Pagès,H., Lin,S.M., Lapointe,D.S. and Green,M.R. (2010) ChIPpeakAnno: a Bioconductor package to annotate ChIP-seq and ChIP-chip data. *BMC Bioinformatics*, **11**, 237.
46. Quinlan,A.R. and Hall,I.M. (2010) BEDTools: a flexible suite of utilities for comparing genomic features. *Bioinformatics*, **26**, 841–842.
47. Gilbert,C., Kristjuhan,A., Winkler,G.S. and Svejstrup,J.Q. (2004) Elongator interactions with nascent mRNA revealed by RNA immunoprecipitation. *Mol. Cell*, **14**, 457–464.
48. Davidson,M.K., Shandilya,H.K., Hirota,K., Ohta,K. and Wahls,W.P. (2004) Atf1-Pcr1-M26 complex links stress-activated MAPK and cAMP-dependent protein kinase pathways via chromatin remodeling of *cgs2*$^{+}$. *J. Biol. Chem.*, **279**, 50857–50863.
49. Yamada,T., Mizuno,K., Hirota,K., Kon,N., Wahls,W.P., Hartsuiker,E., Murofushi,H., Shibata,T. and Ohta,K. (2004) Roles of histone acetylation and chromatin remodeling factor in a meiotic recombination hotspot. *EMBO J.*, **23**, 1792–1803.
50. Sansó,M., Vargas-Pérez,I., Quintales,L., Antequera,F., Ayté,J. and Hidalgo,E. (2011) Gcn5 facilitates Pol II progression, rather than recruitment to nucleosome-depleted stress promoters, in *Schizosaccharomyces pombe*. *Nucleic Acids Res.*, **39**, 6369–6379.
51. Chen,D., Toone,W.M., Mata,J., Lyne,R., Burns,G., Kivinen,K., Brazma,A., Jones,N. and Bähler,J. (2003) Global transcriptional responses of fission yeast to environmental stress. *Mol. Biol. Cell*, **14**, 214–229.
52. Rodríguez-Gabriel,M.A., Burns,G., McDonald,W.H., Martín,V., Yates,J.R., Bähler,J. and Russell,P. (2003) RNA-binding protein Csx1 mediates global control of gene expression in response to oxidative stress. *EMBO J.*, **22**, 6256–6266.
53. Sutani,T., Sakata,T., Nakato,R., Masuda,K., Ishibashi,M., Yamashita,D., Suzuki,Y., Hirano,T., Bando,M. and Shirahige,K. (2015) Condensin targets and reduces unwound DNA structures associated with transcription in mitotic chromosome condensation. *Nat. Commun.*, **6**, 7815.
54. Eshaghi,M., Lee,J.H., Zhu,L., Poon,S.Y., Li,J., Cho,K.H., Chu,Z., Karuturi,R.K.M. and Liu,J. (2010) Genomic binding profiling of the fission yeast stress-activated MAPK Sty1 and the bZIP transcriptional activator Atf1 in response to $H_2O_2$. *PLoS One*, **5**, e11620.
55. Yap,K.L., Li,S., Muñoz-Cabello,A.M., Raguz,S., Zeng,L., Mujtaba,S., Gil,J., Walsh,M.J. and Zhou,M.M. (2010) Molecular interplay of the noncoding RNA *ANRIL* and methylated histone H3 lysine 27 by polycomb CBX7 in transcriptional silencing of *INK4a*. *Mol. Cell*, **38**, 662–674.
56. Wahls,W.P. (1994) RNA associated with a heterodimeric protein that activates a meiotic homologous recombination hot spot: RL/RT/PCR strategy for cloning any unknown RNA or DNA. *PCR Methods Appl.*, **3**, 272–277.
57. Greenall,A., Hadcroft,A.P., Malakasi,P., Jones,N., Morgan,B.A., Hoffman,C.S. and Whitehall,S.K. (2002) Role of fission yeast Tup1-like repressors and Prr1 transcription factor in response to salt stress. *Mol. Biol. Cell*, **13**, 2977–2989.
58. Hirota,K., Hoffman,C.S., Shibata,T. and Ohta,K. (2003) Fission yeast Tup1-like repressors repress chromatin remodeling at the *fbp1*$^{+}$ promoter and the *ade6-M26* recombination hotspot. *Genetics*, **165**, 505–515.
59. Buck,M.J. and Lieb,J.D. (2006) A chromatin-mediated mechanism for specification of conditional transcription factor targets. *Nat. Genet.*, **38**, 1446–1451.
60. Saitoh,S., Mori,A., Uehara,L., Masuda,F., Soejima,S. and Yanagida,M. (2015) Mechanisms of expression and translocation of major fission yeast glucose transporters regulated by CaMKK/phosphatases, nuclear shuttling, and TOR. *Mol. Biol. Cell*, **26**, 373–386.
61. Heiland,S., Radovanovic,N., Hofer,M., Winderickx,J. and Lichtenberg,H. (2000) Multiple hexose transporter of *Schizosaccharomyces pombe*. *J. Bacteriol.*, **182**, 2153–2162.
62. Hao,Z., Furunobu,A., Nagata,A. and Okayama,H. (1997) A zinc finger protein required for stationary phase viability in fission yeast. *J. Cell Sci.*, **110**, 2557–2566.
63. Brandman,O. and Meyer,T. (2008) Feedback loops shape cellular signals in space and time. *Science*, **322**, 390–395.
64. Dunand-sauthier,I., Walker,C.A., Pearce,A.K., Wek,R.C., Tim,C., Narasimhan,J. and Humphrey,T.C. (2005) Stress-activated protein kinase pathway functions to support protein synthesis and translational adaptation in response to environmental stress in fission yeast. *Eukaryot. Cell*, **4**, 1785–1793.
65. Spriggs,K.A., Bushell,M. and Willis,A.E. (2010) Translational regulation of gene expression during conditions of cell stress. *Mol. Cell*, **40**, 228–237.

66. Smitha,R.L. and Johnsonb,A.D. (2000) Turning genes off by Ssn6-Tup1: A conserved system of transcriptional repression in eukaryotes. *Trends Biochem. Sci.*, **25**, 325–330.
67. Rizzo,J.M., Mieczkowski,P.A. and Buck,M.J. (2011) Tup1 stabilizes promoter nucleosome positioning and occupancy at transcriptionally plastic genes. *Nucleic Acids Res.*, **39**, 8803–8819.
68. Cooper,J.P., Roth,S.Y. and Simpson,R.T. (1994) The global transcriptional regulators, *SSN6* and *TUP1*, play distinct roles in the establishment of a repressive chromatin structure. *Genes Dev.*, **8**, 1400–1410.
69. Chen,K., Wilson,M.A., Hirsch,C., Watson,A., Liang,S., Lu,Y., Li,W. and Dent,S.Y.R. (2013) Stabilization of the promoter nucleosomes in nucleosome-free regions by the yeast Cyc8-Tup1 corepressor. *Genome Res.*, **23**, 312–322.
70. Fagerstrom-Billai,F., Durand-Dubief,M., Ekwall,K. and Wright,A.P.H. (2007) Individual subunits of the Ssn6-Tup11/12 corepressor are selectively required for repression of different target genes. *Mol. Cell. Biol.*, **27**, 1069–1082.
71. Weiner,A., Hughes,A., Yassour,M., Rando,O.J. and Friedman,N. (2010) High-resolution nucleosome mapping reveals transcription-dependent promoter packaging. *Genome Res.*, **20**, 90–100.
72. Gilchrist,D.A., Dos Santos,G., Fargo,D.C., Xie,B., Gao,Y., Li,L. and Adelman,K. (2010) Pausing of RNA polymerase II disrupts DNA-specified nucleosome organization to enable precise gene regulation. *Cell*, **143**, 540–551.
73. García,P., Paulo,E., Gao,J., Wahls,W.P., Ayté,J., Lowy,E. and Hidalgo,E. (2014) Binding of the transcription factor Atf1 to promoters serves as a barrier to phase nucleosome arrays and avoid cryptic transcription. *Nucleic Acids Res.*, doi:10.1093/nar/gku704.
74. Soriano,I., Quintales,L. and Antequera,F. (2013) Clustered regulatory elements at nucleosome-depleted regions punctuate a constant nucleosomal landscape in *Schizosaccharomyces pombe*. *BMC Genomics*, **14**, 813.
75. Lam,M.T.Y., Li,W., Rosenfeld,M.G. and Glass,C.K. (2014) Enhancer RNAs and regulated transcriptional programs. *Trends Biochem. Sci.*, **39**, 170–182.
76. Sigova,A.A., Abraham,B.J., Ji,X., Molinie,B., Hannett,N.M., Guo,Y.E., Jangi,M., Giallourakis,C.C., Sharp,P.A. and Young,R.A. (2015) Transcription factor trapping by RNA in gene regulatory elements. *Science*, **350**, 978–981.
77. Hoffman,C.S. and Winston,F. (1989) A transcriptionally regulated expression vector for the fission yeast *Schizosaccharomyces pombe*. *Gene*, **84**, 473–479.
78. Robinson,J.T., Thorvaldsdóttir,H., Winckler,W., Guttman,M., Lander,E.S., Getz,G. and Mesirov,J.P. (2011) Integrative genomics viewer. *Nat. Biotechnol.*, **29**, 24–26.